An Improved Friction Model and Its Implications for the Slip, the Frictional Energy, and the Cornering Force and Moment of Tires

K. -S. Park, C. -W. Oh, T. -W. Kim, Hyun-Yong Jeong*
Department of Mechanical Engineering, Sogang University,
1 Shinsoo-Dong, Mapo-Gu, Seoul 121-742, Korea
Y. -H. Kim
Hankook Tire R&D Center,
23-1 Jang-Dong, Yuseong-Gu, Daejun 305-343, Korea

An improved friction model was proposed with consideration of the effect of the sliding speed, the contact pressure and the temperature, and it was implemented into a user subroutine of a commercial FEM code, ABAQUS/Explicit. Then, a smooth tire was simulated for free rolling, driving, braking and cornering situations using the improved friction model and the Coulomb friction model, and the effect of the friction models on the slip, the frictional energy distribution and the cornering force and moment was analyzed. For the free rolling, the driving and the braking situations, the improved friction model and the Coulomb friction model resulted in similar profiles of the slip and the frictional energy distributions although the magnitudes were different. The slips obtained from the simulations were in a good correlation with experimental data. For the cornering situation, the Coulomb friction model with the coefficient of friction of 1 or 2 resulted in lower or higher cornering forces and moments than experimental data. In addition, in contrast to experimental data it did not result in a maximum cornering force and a decrease of the cornering moment for the increase of the speed. However, the improved friction model resulted in similar cornering forces and moments to experimental data, and it resulted in a maximum cornering force and a decrease of the cornering moment for the increase of the speed, showing a good correlation with experimental data.

Key Words : Tire, Friction Model, Slip, Frictional Energy, Cornering Force, Cornering Moment

1. Introduction

As a tire rotates, a friction force acts between the tire and the road, and the friction force can be expressed as a coefficient of friction multiplied by a normal force. As for the coefficient of friction, the Coulomb friction model has mostly been used. In the Coulomb friction model, the coefficient of friction is assumed to be constant, and the friction force increases linearly as the normal force increases. For some cases, it is also assumed that the friction force is limited by a critical value. However, it is noteworthy that the coefficient of friction is usually not a constant, rather it depends on the slip speed, the contact pressure, the temperature, the contact materials and the contact surface (eg. road) condition (Clark, 1981). Thus, an exponential friction model, in which the coefficient of friction decreases exponentially from the static

* Corresponding Author,
E-mail : jeonghy@sogang.ac.kr
TEL : +82-2-705-8640; **FAX** : +82-2-712-0977
Department of Mechanical Engineering, Sogang University, 1 Shinsoo-Dong, Mapo-Gu, Seoul 121-742, Korea. (Manuscript **Received** January 24, 2006; **Revised** June 7, 2006)

coefficient of friction to the kinetic coefficient of friction as the slip speed increases, was proposed (ABAQUS, 2000). In addition, a power law or a quadratic formula for the coefficient of friction was also proposed, based on friction test data for various slip speeds and contact pressures (Dorsch, 2002).

In general, for a specific combination of the contact materials and the contact surface the coefficient of friction can be expressed as a function of the slip speed, v, after measuring it for various slip speeds. Especially for rubber friction, the temperature can be taken into account through the shift factor, a_T, which can be obtained from the WLF equation (Williams, 1955). Since the friction force between rubber and road results from the hysterestic deformation of rubber over asperities on road, the coefficient of friction and the elastic modulus have the same temperature dependency (Persson, 2001). Thus, the function for the coefficient of friction for rubber at another temperature can be obtained by shifting it by a_T along the log scale speed axis. That is, the coefficient of friction can be expressed as a function of $\log(a_T v)$, which is called a master curve of the coefficient of friction. This means that the effect of the slip speed and that of the temperature on the coefficient of friction can be taken into account altogether. Moreover, it has been well known that the coefficient of friction decreases as the contact pressure increases; it is inversely proportional to the contact pressure raised to the power of about 1/3 for a smooth road or about 1/9 for a rough road (Clark, 1981). Thus, the dependency of the coefficient of friction on the slip speed, the temperature and the contact pressure can be expressed by the function of $\log(a_T v)$ multiplied by the ratio of the contact pressure to the reference pressure raised to an exponent, eg. 1/3 or 1/9. This functional form of the coefficient of friction was proposed and successfully used for tire simulations by two authors of this paper (Lee, 2001). In this paper, the same functional form with a difference master curve was used and it was named an improved friction model.

The finite element method (FEM) has long been used for tire response simulations and tire design (Gall, 1995; Goldstein, 1996; Wang, 1996; Kao, 1997; Wu, 1997; Kabe, 2000). Recently, dynamic responses of tires were analyzed by using an explicit FEM code such as LS-DYNA3D, FCRASH, and PAM-CRASH (Kao, 1997; Wu, 1997; Kabe, 2000). Note that static responses of tires can also be analyzed by using an explicit FEM code in a way that an average value taken from a stable region of a response is assumed to be a static response (Kabe, 2000). However, in all the computational simulations mentioned above only the Coulomb friction model was used, and the effect of the slip speed, the contact pressure or the temperature on friction was not taken into account. Dorsch et al. used a power law or a quadratic formula for friction for tire simulations using an implicit FE code (Dorsch, 2002).

In this paper, the improved friction model was first implemented into a user subroutine for friction, VFRIC, in a commercial explicit FEM code, ABAQUS/Explicit, and then a smooth tire was simulated for free rolling, driving, braking and cornering situations using the improved friction model or the Coulomb friction model. As in a previous study (Kabe, 2000), a steady-state solution was obtained from a stable region of the solution. Then, the effect of the friction models on tire responses such as the slip, the frictional energy distribution, and the cornering force and moment was analyzed. For free rolling, driving and braking situations, the profiles of the longitudinal slip and the frictional energy distribution did not change significantly by using one of the two friction models. However, as the torque changed either up to +500 Nm or down to −500 Nm, the profiles as well as the magnitudes of the longitudinal slip and the frictional energy distribution changed drastically. Especially, the longitudinal slips for a torque of 0 Nm, +250 Nm and −250 Nm were compared and proven to be in a good correlation with test data (Clark, 1981).

For cornering testing, a smooth tire was driven at 10 km/h or 65 km/h on a flat surface tire test machine, and the cornering force and moment were measured for several slip angles; they were measured up to the slip angle of 14° at 65 km/h, but they were measured only up to the slip angle

of 6° at 10 km/h because the tire did not slip rather it was scraped at high slip angles. The test data measured at 65 km/h showed that as the slip angle increased, the cornering force increased and then decreased slightly over the slip angle of 8°, and the cornering moment increased and decreased sharply over the slip angle of 4°. In addition, as the speed increased from 10 km/h to 65 km/h, the cornering force increased slightly, but the cornering moment decreased noticeably at the slip angle of 4°. For the cornering simulations, the friction models affected significantly the cornering force and moment. In general, the Coulomb friction model with the coefficient of 1 or 2 resulted in lower or higher cornering forces and moments than the test data, and the cornering force monotonically increased as the slip angle increased. In addition, the Coulomb friction model did not resulted in the decrease of the cornering moment for the increase of the speed. However, the improved friction model resulted in cornering forces and moments similar to the test data, and the cornering force increased and decreased slightly as the slip angle increased. In addition, it resulted in the decrease of the cornering moment for the increase of the speed. That is, the results obtained by using the improved friction model were in a better correlation with the test data than those obtained by using the Coulomb friction model.

2. An Improved Friction Model and Its Implementation

2.1 Friction models

In the Coulomb friction model, the coefficient of friction is a constant regardless of the slip speed, the contact pressure and the temperature. In the exponential friction model, the coefficient of friction decreases exponentially from the static value to the kinetic value as the slip speed increases, and it is expressed as follows.

$$\mu=\mu_k+(\mu_s-\mu_k)\,e^{-d_c v} \tag{1}$$

Here, μ_s is the static coefficient of friction, μ_k is the kinetic coefficient of friction, and d_c is the decay constant.

Note that the dependency of the coefficient of friction on the slip speed, the contact pressure and the temperature can not be taken into account in the Coulomb friction model, and the dependency of the coefficient of friction on the contact pressure and the temperature can not be taken into account in the exponential friction model. In addition, the coefficient of friction usually increases and then decreases as the slip speed increases in contrast to the exponential friction model (Clark, 1981). Therefore, a friction model, in which the effect of the slip speed, the contact pressure and the temperature was taken into account, was proposed by two authors of this paper (Lee, 2001).

First, for a specific combination of contact materials and road condition, the master curve of the coefficient of friction can be expressed as a function of $\log(a_T v)$. The shift factor, a_T, can be obtained from the WLF equation, which is given as follows (Williams, 1955).

$$\log a_T=\frac{-8.86(T-T_s)}{T-T_s+101.6} \tag{2}$$

Here, T is the temperature in usage in ℃ and T_s is the reference temperature in ℃, which is the glass transition temperature plus 50℃. From Eq. (2), the shift factor was easily determined to be 0.00158 around room temperature 25℃ for natural rubber of T_s equal to −22℃. The master curve is shown in Fig. 1 as a solid line along with two dotted lines of coefficient of friction of 1 or 2. The

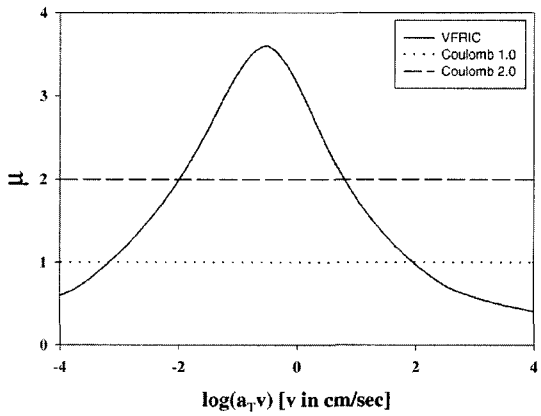

Fig. 1 The coefficient of friction used in the improved friction model (solid line) and in the Coulomb friction model (dotted line)

general profile of the master curve was found in the literature (Clark, 1981), and the dotted lines were set at 1 and 2 around the medium value of the solid curve.

Second, the effect of the contact pressure was taken into account as follows.

$$\mu=(p/p_o)^{-n}f(\log(a_T v)) \tag{3}$$

Here, p is the contact pressure, p_o is the reference contact pressure, n is the exponent which usually depends on the road condition, and f represents a master curve such as the solid curve shown in Fig. 1. When the contact pressure, p, was less than the reference contact pressure, p_o, p was set to be equal to p_o. In addition, p_o was set to be 1.5×10^5 Pa because the coefficient of friction is almost independent of the contact pressure around this value (Persson, 2001), and n was set to be 1/9 because the track on the flat surface tire test machine used in this study was kind of rough. Eq. (3) is the function of the coefficient of friction proposed in this paper in which the effect of the sliding speed, the temperature and the contact pressure is taken into account. However, it is noteworthy that for a different road condition or for a different pair of contact materials, the exponent n and the function f should be set up differently.

2.2 Implementation of the improved friction model

The improved friction model was implemented in the user subroutine for friction called VFRIC in ABAQUS/Explicit (ABAQUS, 2000). The main program passes the slip increment of every node in the contact zone, the normal force acting on the node, the surface area associated with the node and the time increment to VFRIC. Thus, it was possible to calculate the slip speed and the contact pressure at each node in the contact zone, and subsequently to calculate the coefficient of friction by using Eq. (3) and finally to calculate the frictional force acting at each node. It was also possible to calculate the frictional energy from a dot product of the frictional force and the slip increment. In addition, the longitudinal slip, i.e. the summation of the slip increment, and the frictional energy of each node in the contact zone were defined as state variables, and they could be updated at every time increment.

3. Tire Simulations

3.1 Free rolling, driving and braking simulations

A smooth tire (185/65R14) was simulated for free rolling, driving and braking situations. The finite element model of the tire with the global and local coordinate systems was shown in Fig. 2. It consisted of 8-node solid elements and 4-node membrane elements. In addition, rubber was modeled as a viscoelastic material with long term Young's modulus of 4.7×10^6 Pa, Poisson's ratio of 0.49 and four Prony series parameters, and the carcass and the belts were modeled as reinforcement fibers using the REBAR option in ABAQUS. The membrane of the carcass was modeled as an elastic material with Young's modulus of 3.5×10^6 Pa and Poisson's ratio of 0.49, and the cord of the carcass was modeled with Young's modulus of 3.9×10^9 Pa and Poisson's ratio of 0.3. In addition, the membrane of the belts was modeled with Young's modulus of 5.5×10^6 Pa and Poisson's ratio of 0.49, and the cord of the belts was

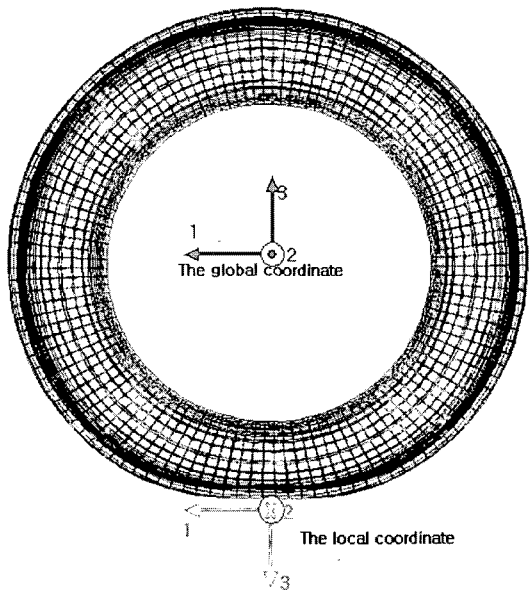

Fig. 2 A smooth tire model in the global and the local coordinate systems

modeled with Young's modulus of 8.4×10^{10} Pa and Poisson's ratio of 0.3. However, the carcass and the belts could have been modeled as anisotropic elastic materials of which the properties were obtained from the Halpin-Tsai equations and a tensor transformation (Berthelot, 1997).

For the simulations, the tire was inflated by 2.06×10^5 Pa from $t=0$ sec and subjected to a load of 6080 N from $t=0.02$ sec. Then, the tire was accelerated from $t=0.1$ sec to $t=0.2$ sec, after which the speed was set at 10 km/h for the free rolling situation. The speed being set at 10 km/h, a torque of ±250 Nm or ±500 Nm was applied at the center of the tire for the driving or the braking situation. Only after the tire response became stable, the average value of a simulation result was taken and it was regarded as a steady-state solution ; the average value was taken from $t=1$ sec to $t=1.5$ sec for the speed of 10 km/h or from $t=0.5$ sec to $t=0.75$ sec for the speed of 65 km/h. For the simulations, the time increment was slightly over 1×10^{-6} sec.

From the user subroutine for friction, VFRIC, the longitudinal slip increment and the longitudinal slip of a node, and the frictional energy acting on a node could be obtained while the node passed through the contact zone. Since the longitudinal slip is the summation of the longitudinal slip increment, it is the total slip of a node from the initial contact with the road. The longitudinal slip increment, the longitudinal slip and the frictional energy distribution obtained using the Coulomb friction model with the coefficient of friction of 1 are shown in Fig. 3(a), (b) and (c), respectively, and those obtained using the improved friction model are shown in Fig. 4(a), (b) and (c), respectively. Note that the frictional energy distribution over the contact zone could be shown clearly by drawing the frictional energy of a row of nodes in the lateral direction while they passed through the contact zone. As shown in Figs. 3(a) and 4(a), the longitudinal slip increment was positive at the leading zone, negative around the center and the trailing zone, but it became positive again at the trailing edge. Thus, the longitudinal slip increased, decreased and then slightly increased as shown in Figs. 3(b) and 4(b). In addition, the frictional energy distribution was moderate at the leading zone, around the center and at the trailing edge as shown in Figs. 3(c) and 4(c). Note that the frictional energy distribution was similar to the absolute value of the

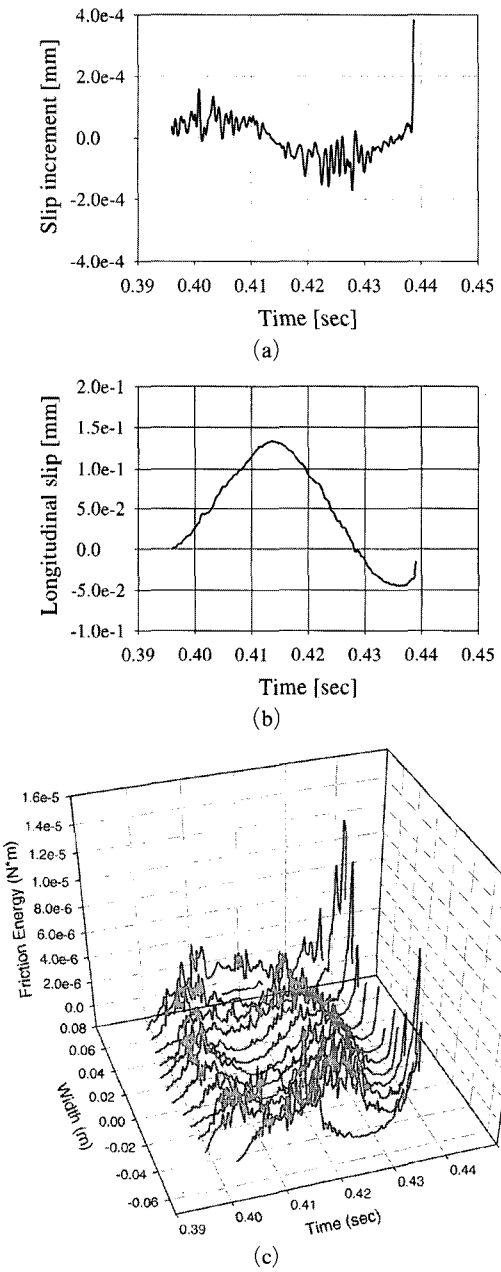

Fig. 3 (a) Longitudinal slip increment (b) Longitudinal slip (c) Frictional energy distribution for the free rolling obtained using the Coulomb friction model

longitudinal slip increment, and the profiles of the longitudinal slip increment, the longitudinal slip and the frictional energy distribution obtained using the improved friction model were similar to those obtained using the Coulomb friction model although the magnitudes were different. Thus, for the driving situation under a torque of 250 Nm and the braking situation under a torque of −250 Nm, only the simulation results obtained using the improved friction model were shown in Fig. 5

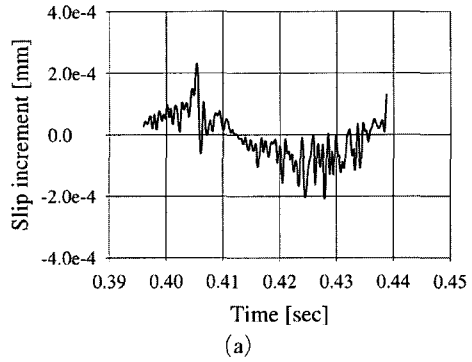

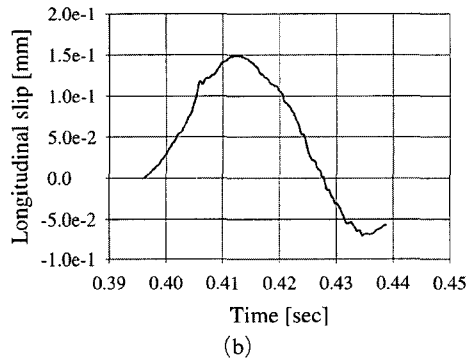

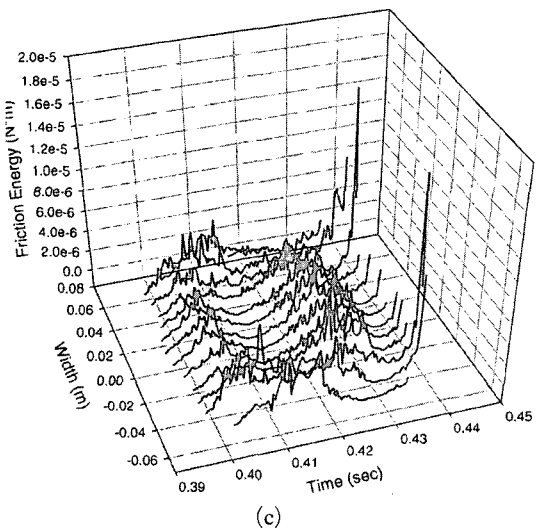

Fig. 4 (a) Longitudinal slip increment (b) Longitudinal slip (c) Frictional energy distribution for the free rolling obtained using the improved friction model

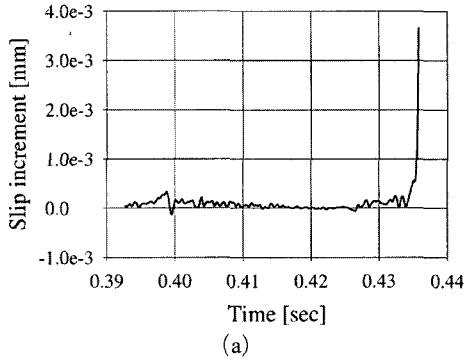

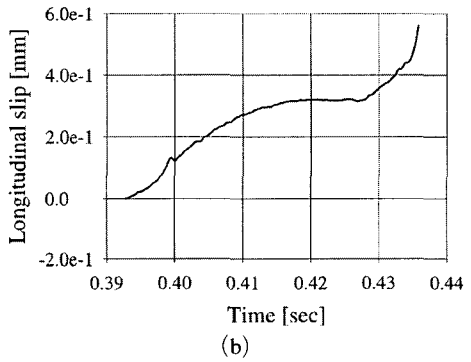

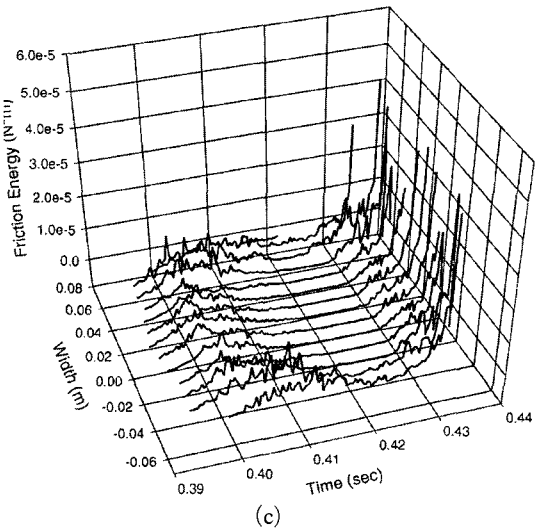

Fig. 5 (a) Longitudinal slip increment (b) Longitudinal slip (c) Frictional energy distribution for the driving under a torque of 250 Nm obtained using the improved friction model

and in Fig. 6, respectively.

For the driving situation, the longitudinal slip increment was positive at the leading zone, close to zero around the center, and highly positive at the trailing edge as shown in Fig. 5(a). Thus, the longitudinal slip increased gradually from the leading edge to the center, leveled off to the trailing zone, and increased rapidly at the trailing edge as shown in Fig. 5(b). In addition, the frictional energy distribution was moderate at the leading zone, and high at the trailing edge, but it was almost zero at the center as shown in Fig. 5(c). For the braking situation, the longitudinal slip increment was positive at the leading zone, crossed zero before the center, and negative at the center and the trailing zone as shown in Fig. 6(a). Thus, the longitudinal slip increased slightly at the leading zone, decreased almost steadily before the center to the trailing edge as shown in Fig. 6(b). In addition, the frictional energy distribution was low at the leading zone, but it was high at the center and the trailing zone as shown in Fig. 6(c).

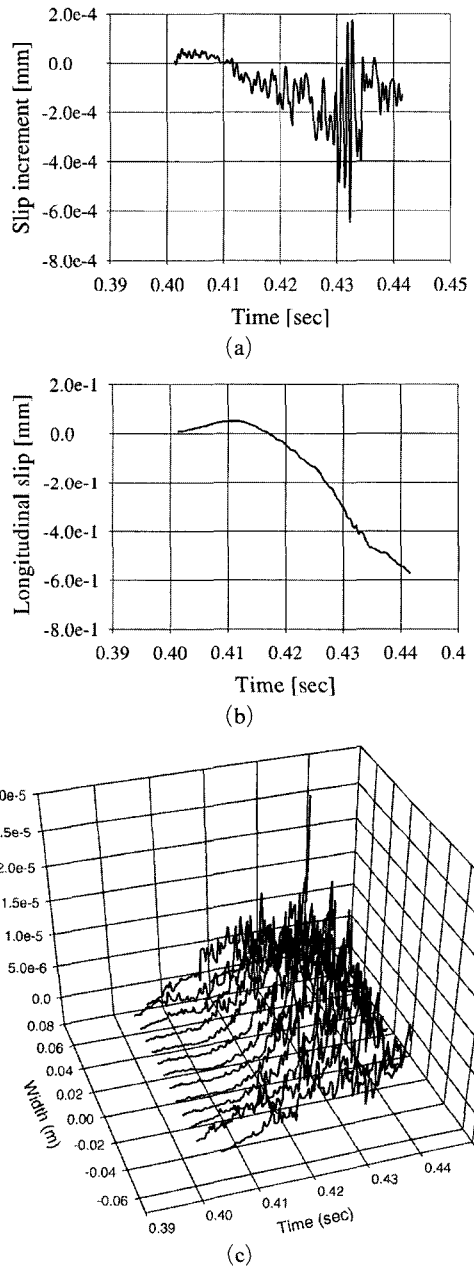

Fig. 6 (a) Longitudinal slip increment (b) Longitudinal slip (c) Frictional energy distribution for the braking under a torque of −250 Nm obtained using the improved friction model

The driving situation under a torque of 500 Nm was also simulated, and the results were similar to those under a torque of 250 Nm except that the magnitudes were bigger, the longitudinal slip increment was not as close to zero around the center as the case of 250 Nm, and consequently the longitudinal slip did not level off at the center rather increased gradually. The braking situation under a torque of −500 Nm was also simulated, and the results were similar to those under a torque of −250 Nm except that the magnitudes were bigger, the longitudinal slip increment was always negative, and consequently the longitudinal slip never became positive, decreasing slowly before the center but decreasing rapidly toward the trailing edge. In addition, the profile of the frictional energy distribution under a torque of 500 Nm or −500 Nm was almost the same as that under a torque of 250 Nm or −250 Nm although the magnitude was bigger.

It is noteworthy that the profiles of the longitudinal slip for the free rolling, the driving and the braking situations shown in Fig. 3(b) (or Fig. 4(b)), Figs. 5(b) and 6(b), respectively, are similar to the corresponding experimental data (Clark, 1981). In addition, the longitudinal slip and the friction energy distribution changed drastically as the torque changed to ±250 Nm or ±500 Nm. For a given material, the frictional energy is

related to the amount of wear; the higher frictional energy is, the more wear occurs. Therefore, a different frictional energy distribution for each driving situation implies for a different wear pattern and amount.

3.2 Cornering simulations

As shown in Fig. 7, a smooth tire was rotated with respect to the axle, and at the same time it was translated in the lateral direction to simulate a cornering situation with slip. The angular and the lateral speeds of the tire were set in a way that the resultant speed of the tire remained at 10 km/h or 65 km/h. That is, as the lateral speed increased, the angular speed of the tire decreased accordingly. By increasing the lateral speed of the tire, the slip angle, α, i.e. the angle between the longitudinal velocity and the resultant velocity, could be increased.

For the cornering simulations, the slip angle was set at 1°, 2° or every 2° thereafter, and the cornering force and moment were obtained using the Coulomb friction model with the coefficient of friction of 1 or 2 or using the improved friction model. The cornering force is a resultant reaction force, and the cornering moment is a reaction moment acting with respect to the vertical axis. In addition, the cornering force and moment for the smooth tire were measured at a flat surface tire test machine. The slip angle was increased up to only 6° for the speed of 10 km/h because the tire did not slip rather it was scraped over the slip angle of 6°, but it was increased up to 14° for the speed of 65 km/h. The cornering force and moment for the speed of 10 km/h obtained both from the simulations and from the tests are shown in Fig. 8(a) and (b), and those for the speed of 65 km/h are shown in Fig. 9(a) and (b). The test data shown in Fig. 9(a) and (b) indicate that the cornering force increased gradually to its maximum occurring around the slip angle of 8° and decreased slightly thereafter, and the cornering moment increased to its maximum occurring around the slip angle of 4° and decreased rapidly thereafter. As the speed increased from 10 km/h to 65 km/h, the cornering force increased slightly because the centrifugal force increased and conse-

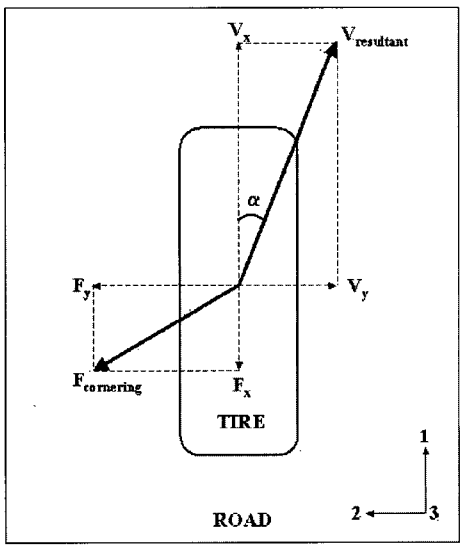

Fig. 7 The slip angle and the cornering force in the cornering situation

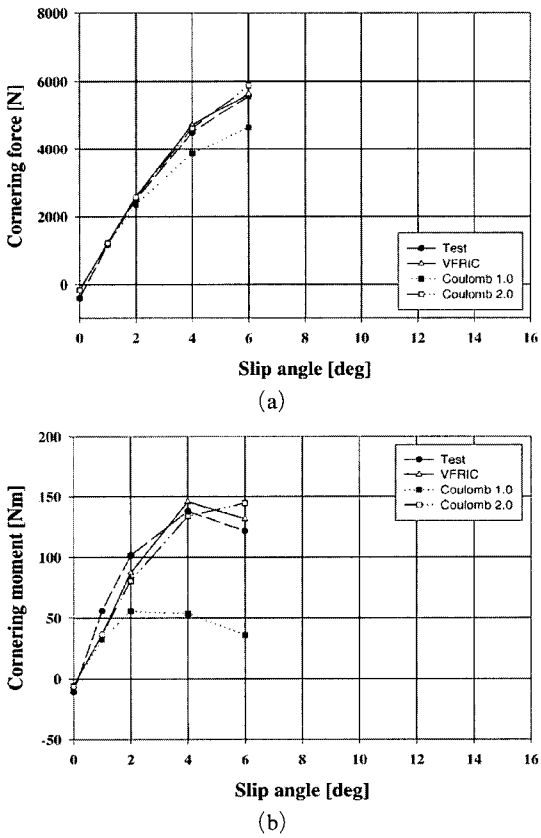

Fig. 8 (a) Cornering force (b) Cornering moment for the speed of 10 km/h

quently the contact force increased. However, as the speed increased from 10 km/h to 65 km/h, the cornering moment at the slip angle of 4° decreased by 18% because the slip speed at the trailing zone increased and consequently the coefficient of friction as well as the friction force decreased. In other words, the moment arm, so called the pneumatic trail, decreased from 31.5 mm to 23.5 mm although the cornering force increased.

The cornering force and moment obtained using the Coulomb friction model with the coefficient of friction of 1 or 2 were close to the test data at low slip angles of up to 1° or 2°. However, at medium and high slip angles they were lower in the case of the coefficient of friction of 1 than the test data, and they were higher in the case of the coefficient of friction of 2. It is noteworthy that the Coulomb friction model did not result in a maximum cornering force, but it resulted in a monotonically increasing cornering force. In addition, the Coulomb friction model did not result in the decrease of the cornering moment for the increase of speed from 10 km/h to 65 km/h. However, the improved friction model resulted in a maximum cornering force occurring around the slip angle of 10°, and it also resulted in the decrease of the cornering moment for the increase of speed. There are still some differences between the simulation results obtained using the improv-

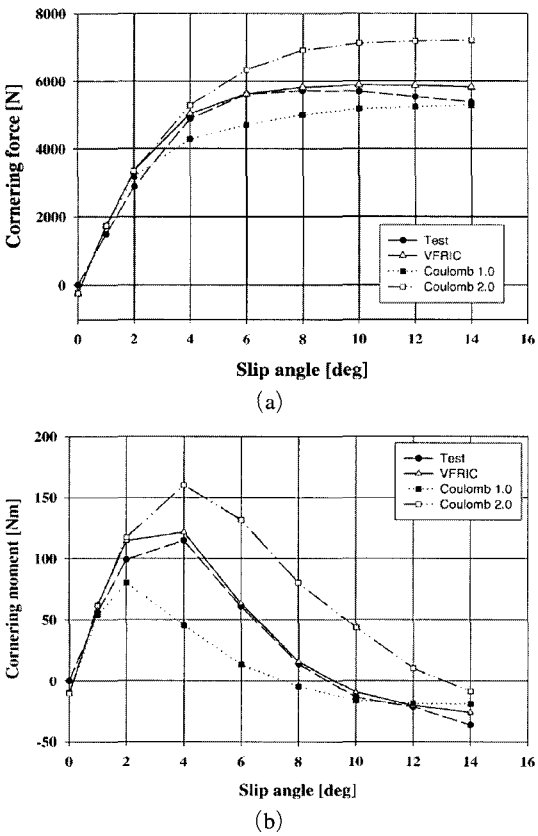

Fig. 9 (a) Cornering force (b) Cornering moment for the speed of 65 km/h

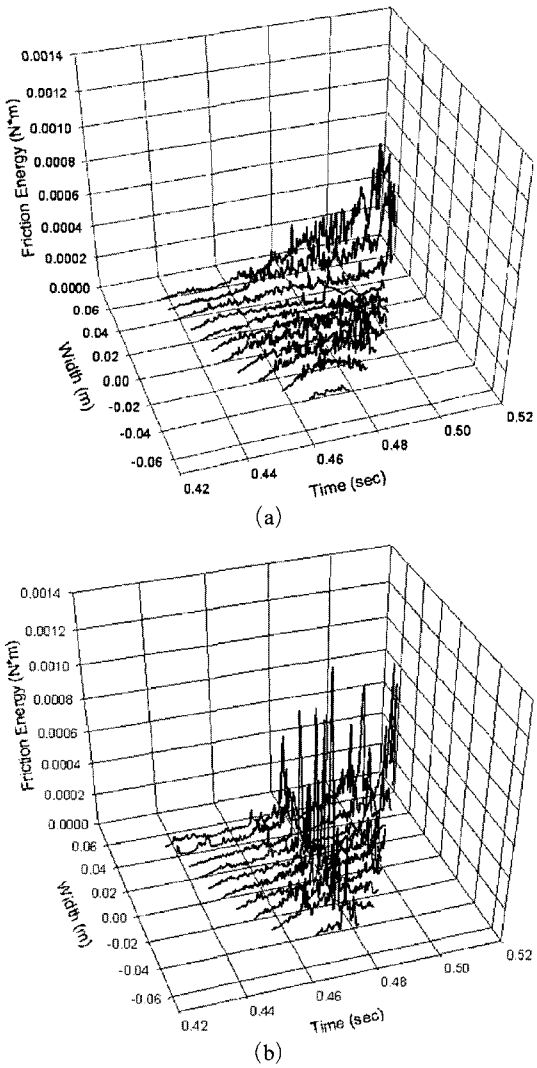

Fig. 10 (a) Frictional energy distribution obtained using the Coulomb friction model for the slip angle of 6° (b) Frictional energy distribution obtained using the improved friction model for the slip angle of 6°

ed friction model and the test data, but the improved friction model showed a better correlation with the test data than the Coulomb friction model with the coefficient of friction of 1 or 2.

The frictional energy distribution for the slip angle of 6° obtained using the Coulomb friction model with the coefficient of friction of 2 and that obtained using the improved friction model were shown in Fig. 10(a) and (b), respectively. The frictional energy increased gradually from the leading edge to the trailing edge when the Coulomb friction model was used, but it was high at the center of the contact zone and the trailing edge when the improved friction model was used. For the sake of brevity, the frictional energy distributions for other slip angles were not shown because the trend was the same. However, the two different friction models resulted in different cornering forces and moments as well as frictional energy distributions, implying for different tire characteristics and wear patterns during cornering with slip.

4. Conclusions

An improved friction model, in which the effect of the sliding speed, the contact pressure and the temperature can be taken into account, was proposed in this paper, and then it was implemented into a user subroutine for friction, VFRIC, provided in ABAQUS/Explicit 5.8 or above. The friction model was successfully used in the analysis of the slip and the frictional energy distribution for the free rolling, driving and braking situations and in the analysis of the cornering force and moment and the frictional energy distribution for the cornering situation.

The simulations for the free rolling, the driving and the braking situations indicated that when a different friction model was used for the same situation, the magnitudes of the longitudinal slip and the subsequent friction energy distribution were different, but the profiles were almost the same. However, the profiles as well as the magnitudes changed drastically as the torque changed, and these different friction energy distributions implied for different wear patterns and amounts. It is noteworthy that the longitudinal slip profiles obtained from the simulations were in a good correlation with experimental data (Clark, 1981).

For the cornering simulations, the Coulomb friction model and the improved friction model resulted in different cornering forces and moments. The Coulomb friction model resulted in either a higher or lower cornering force and moment, and it did not show a maximum cornering force. In addition, the Coulomb friction model did not show a decrease of the cornering moment for the increase of the speed. However, the improved friction model resulted in a maximum cornering force, and it also showed a decrease of the cornering moment for the increase of the speed. That is, the improved friction model resulted in a better correlation with the test data. Therefore, it can be concluded that it is necessary to consider the effect of slip speed, the contact pressure and temperature for tire and other rubber contact simulations.

Acknowledgements

The tests were conducted at the R&D center of Hankook Tire Co., and this is highly appreciated.

References

ABAQUS, 2000, *User's Manual, Hibbit*, Karlsson & Sorenson, Inc., Version 5.8.

Berthelot, J.-M., 1997, *Composite Materials Mechanical Behavior and Structural Analysis*, Springer.

Clark, S. K., 1981, *Mechanics of Pneumatic Tires*, U. S. Department of Transportation, NHTSA, Washington D. C., DOT HS805-952.

Dorsch, V., Becker, A. and Vossen, L., 2002, "Enhanced Rubber Friction Model for Finite Element Simulations of Rolling Tires," *Plastics, Rubber and Composites*, Vol. 31, pp. 458~464.

Gall, R., Tabaddor, F., Robbins, D., Majors, P., Sheperd, W. and Johnson, S., 1995, "Some Notes on the Finite Element Analysis of Tires," *Tire Science and Technology*, TSTCA, Vol. 23, No. 3, July-September, pp. 175~188.

Goldstein, A. A., 1996, "Finite Element An-

alysis of a Quasi-Static Rolling Tire Model for Determination of Truck Tire Forces and Moments," *Tire Science and Technology*, TSTCA, Vol. 24, No. 4, October-December, pp. 278~293.

Kabe, K. and Koishi, M., 2000, "Tire Cornering Simulation Using Finite Element Analysis," *Journal of Applied Polymer Science*, Vol.78, pp.1566~1572.

Kao, B. G. and Muthukrishnan, M., 1997, "The Transient Analysis with an Explicit Finite Element Program," *Tire Science and Technology*, TSTCA, Vol. 25, No. 4, October-December, pp. 230~244.

Lee, D. -J., Nahm, S. -W., Jeong, H. -Y. and Kim, Y. -H., 2001, "A New Friction Model and Its Implications for the Frictional Energy and the Contact Forces," 20th Annual Meeting and Conference on Tire Science and Technology.

Persson, B. N. J., 2001, "Theory of Rubber Friction and Contact Mechanics," *Journal of Chemical Physics*, Vol. 115, pp. 3840~3861.

Wang, T. -M, Daniel, I. M. and Huang, K., 1996, "Stress Analysis of Tire Sections," *Tire Science and Technology*, TSTCA, Vol. 24, No. 4, October-December, pp. 349~366.

Williams, M. L., Landel, R. F. and Ferry, J. D., 1955, *Journal of American Chemistry Society*, Vol. 77, p. 3701.

Wu, S. R., Gu, L. and Chen, H., 1997, "Airbag Tire Modeling by the Explicit Finite Element Method," *Tire Science and Technology*, TSTCA, Vol. 25, No. 4, October-December, pp. 288~300.